Available online at www.sciencedirect.com
SCIENCE DIRECT®
Journal of Catalysis 240 (2006) 245–257
JOURNAL OF CATALYSIS
www.elsevier.com/locate/jcat

Synthesis, characterisation, catalytic activity and structural stability of $LaCo_{1-y}Fe_yO_{3\pm\lambda}$ perovskite catalysts for combustion of ethanol and propane

Nora A. Merino [a], Bibiana P. Barbero [a], Patricio Ruiz [b], Luis E. Cadús [a,*]

[a] *Instituto de Investigaciones en Tecnología Química (INTEQUI), UNSL-CONICET, Casilla de Correo 290, 5700 San Luis, Argentina*
[b] *Université Catholique de Louvain, Place Croix du Sud 2, Boite 17, 1348 Louvain la Neuve, Belgium*

Received 7 February 2006; revised 24 February 2006; accepted 26 March 2006

Abstract

$LaCo_{1-y}Fe_yO_3$ perovskite-type oxides with $y = 0.1$, 0.3, and 0.5 were prepared by the citrate method and characterized by X-ray diffraction (XRD), BET surface area measurement (SSA), diffuse reflectance infrared Fourier transform spectroscopy (DRIFTS), X-ray photoelectron spectroscopy (XPS), temperature-programmed reduction (TPR), and Mössbauer spectroscopy. With this preparation method, a good inclusion of the substituting cation in the B-site is reached, maintaining the rhombohedral crystalline structure, modifying the volume of the unit cell, and weakening the B–O bond. This likely affects the capacity and the mechanism of oxygen supply or the redox behavior. At high iron content, Fe^{4+} could exist. Surface enrichment in lanthanum was observed on XPS. The singularity observed in the improvement of the catalytic activity for $y = 0.1$, in both propane and ethanol combustion, could be explained by the electronic complexity introduced by iron in the perovskite conductor characteristics.

Keywords: Perovskites; Cobalt; Iron; Citrate method; Catalytic oxidation; Ethanol; Propane

1. Introduction

ABO_3 perovskite-type oxides, whose main characteristic is a well-defined structure, have demonstrated to be excellent catalysts for volatile organic compound (VOC) combustion [1,2]. Both A and B cations can be partially substituted, leading to a $A_{1-x}A'_xB_{1-y}B'_yO_{3\pm\lambda}$ general formula. The partial substitution of A′ for A of different oxidation states leads to the formation of vacancies of the crystalline bonds and also to stabilization of unusual oxidation states of the B cation [2]. The B partial substitution by a B′ cation can promote changes on both the redox ion couples and the active sites, as well as on the stability of the crystalline structure [3], even at high temperatures. By definition, the perovskite structure functions as a host structure that, according to the substituting cations, can exhibit different semiconductor behaviors.

The preparation method is important both in defining suitable textural characteristics for catalysis and in achieving phases of great purity. The literature describes numerous synthesis methods, most of which involve synthesizing materials for applications other than catalysis and allow incorporation of cations into the functional perovskite structure due to the high calcination temperatures used.

Several techniques have been developed to address the problem of perovskite purity; the most commonly used of these is the sol–gel citrate method [4]. This method makes it possible to obtain catalysts of high surface area, but it has the drawback of rather rapid sintering depending on the temperature. Other methods also have been used, including that reported by Kaliaguine et al. [5], who synthesized $LaCoO_3$ and $LaCoFeO_3$ perovskites by a mechano-synthesis method involving mixing the reactants using additives.

Recently, using the citrate method and carefully controlling the synthesis parameters, we synthesized $La_{1-x}Ca_xCoO_{3\pm\lambda}$ perovskites with appropriate texture and excellent catalytic

* Corresponding author. Fax: +54 2652 426711.
E-mail address: lcadus@unsl.edu.ar (L.E. Cadús).

0021-9517/$ – see front matter
doi:10.1016/j.jcat.2006.03.020

performance in VOC combustion [6]. $La_{1-x}Ca_xCoO_{3\pm\lambda}$ perovskites demonstrate excellent structural stability under catalytic test conditions. Neither specific surface area collapse nor structural change was observed. Although only very slight deactivation was observed, this could be avoided entirely by changing the hydrocarbon/oxygen ratio in the feed.

The addition of another A′ cation, such as Ce, in $La_{0.9}Ce_{0.1}Co_{1-x}Fe_xO_{3\pm\lambda}$ perovskite showed that for $x \leqslant 0.2$, it is not possible to obtain the perovskite structure but is possible to obtain the spinel structure [7]. In addition, Barbero et al. [8], working with $La_{1-x}Ca_xFeO_{3\pm\lambda}$ perovskites, found that even if the catalytic performance is not as great as that of the $La_{1-x}Ca_xCoO_3$ catalysts reported previously [6], they did demonstrate excellent structural stability, and the citrate method is simple and appropriate for obtaining single phases avoiding segregation and/or contamination.

The effect of the nature of the B cation on the physicochemical and catalytic properties of lanthanum-based perovskites has been widely studied, and those containing Mn, Co, or Fe have been found to be the most active in VOC combustion [1,9–11]. According to the kinetic model proposed for hydrocarbon activation, weakly adsorbed oxygen is involved in the reaction at low temperature, whereas lattice oxygen becomes reactive at high temperature [1]. Perovskite stability is closely related to both the perovskite crystalline system and the calcination temperature. $LaCoO_3$ is rhombohedral and $LaFeO_3$ is orthorhombic; therefore, it appears to be of interest to correlate the structural stability and redox properties of $LaB_1B_2O_3$ (B_1 = Co, B_2 = Fe) perovskites with their catalytic activity in propane and ethanol combustion. Note that the oxidation reactivity of the volatile organic compounds is in the following order: alcohols > aldehydes > aromatics > ketones > alkenes > alkanes [12,13]. Because of this, it is important and of great interest to study and compare the catalytic activity in alkanes, which are the less reactive, and alcohols, which are more reactive.

What we observed in previous work [6,8], as well as what has been reported about the stability by Fierro et al. [14] for perovskites with B = Ni when this is substituted with Fe, have contributed to the idea behind the present paper. In fact, the addition of Fe in the $La_{1-x}Ca_xCoO_3$ structure can be an interesting factor in stabilization. Nevertheless, and with the aim of observing the influence of Fe without any interference from Ca, this work reports on structural studies, stability studies, and the catalytic consequences of the $LaCo_{1-y}Fe_yO_{3\pm\lambda}$ system.

2. Experimental

2.1. Catalyst preparation

$LaCo_{1-y}Fe_yO_3$ (y = 0.1, 0.3, 0.5) perovskites were prepared by the citrate method [4]. $La(NO_3)_3{\cdot}6H_2O$ (Fluka, 99%), $Co(NO_3)_2{\cdot}6H_2O$ (Acros Organics 99%), $Fe(NO_3)_3{\cdot}9H_2O$ (Aldrich, 98%), and citric acid (Merck 99.5%) were used as reagents. An aqueous solution of citric acid with a 10% excess over the number of ionic equivalents of cations was prepared. The aqueous solutions of the metal nitrates were added to that of citric acid, and they were agitated for 15 min. The resulting solution was concentrated by slowly evaporating water under vacuum in a rotavapor at 75 °C until a gel was obtained. This gel was dried in an oven, with the temperature increased slowly up to 200 °C and maintained there overnight, to produce a solid amorphous citrate precursor. The resulting precursor was milled and then calcined in air at 700 °C for 2 h.

2.2. Catalyst characterization

2.2.1. BET specific surface area measurements

The specific surface area (SSA) of the catalysts was calculated by the BET method from the nitrogen adsorption isotherms obtained at 77 K on 200 mg of sample outgassed at 250 °C using a Micromeritics ASAP 2000 apparatus.

2.2.2. X-Ray diffraction

To monitor the evolution of the crystallinity, X-ray diffraction (XRD) patterns of the precursors were obtained at room temperature, at 200 °C, and then at 50 °C increments up to 700 °C, with the patterns recorded after exposing the sample for 1 h at each temperature. A Siemens diffractometer operated at 40 kV and 40 mA with a monochromator and Cu-K_α radiation (λ = 0.15418 nm) was used. The data were collected at 0.02° at a counting time of 2 s per step, in the (2θ) range of 20°–90°.

XRD patterns of the catalysts calcined at 700 °C were recorded at room temperature using a Rigaku diffractometer operated at 30 kV and 20 mA with Ni-filtered Cu-K_α radiation (λ = 0.15418 nm). The data were collected at 0.02° at a counting time of 5 s per step, in the (2θ) range of 20°–90°. In both cases, the crystalline phases were identified by reference to the powder XRD data (JCPDS-ICDD) using standard spectra software.

2.2.3. Diffuse reflectance infrared Fourier transform spectroscopy

Diffuse reflectance infrared Fourier transform spectroscopy (DRIFTS) spectra were collected with a Brüker EQUINOX55 infrared spectrometer equipped with a cooled-air MIR source with KBr optics and a MCT detector. The samples were placed inside an environmental temperature-controlled chamber (Spectra-Tech 0030–103) equipped with SeZn windows and attached to a diffuse reflectance accessory (Spectra-Tech collector). The spectrum of an aluminium mirror was used as background. All of the spectra (200–800 scans with 4-cm^{-1} resolution) were recorded in helium atmosphere at room temperature (after 1 h of helium flushing) or at 250 °C (after 30 min of stabilization at this temperature). The spectra are presented in absorbance mode without any manipulation. The helium flow was passed through a water trap (gas purifier, Alltech) before being admitted into the analysis cell. In addition, analysis under CO_2/He was performed over $LaCo_{0.9}Fe_{0.1}O_3$ with the sample kept for 1 h at each of the following temperatures: 150, 250, and 350 °C.

2.2.4. X-Ray photoelectron spectroscopy

X-Ray photoelectron spectroscopy (XPS) analyses were performed on a Surface Science Instruments SSX 100/206 photoelectron spectrometer with a monochromatized microfocused Al X-ray source. Spectra were registered after the samples were purged at room temperature in vacuum. The residual pressure in the analysis chamber during the analysis was about 10^{-6} Pa. The flood gun energy was adjusted at 10 eV. The following spectra were recorded: survey spectrum, C_{1s}, O_{1s}, La_{3d}, Co_{2p}, Fe_{2p}, and C_{1s} again to check the stability of charge compensation in function of time. The data treatment was performed with appropriate software. Binding energies were calibrated with respect to the C-(C,H) component of the C_{1s} peak fixed at 284.8 eV. The atomic ratios were calculated using the atomic sensitivity factors provided by the manufacturer.

2.2.5. Temperature-programmed reduction

Temperature-programmed reduction (TPR) experiments were performed in a quartz reactor with a thermal conductivity detector. In these experiments, 50-mg samples were pretreated with helium gas, with the temperature increased from room temperature up to 700 °C at a rate of 10 °C min^{-1} and then cooled to 50 °C. The reducing atmosphere was a 5% H_2/N_2 mixture at a total flow rate of 30 mL min^{-1}. The temperature was increased at a rate of 10 °C min^{-1} from 50 °C up to about 725 °C.

2.2.6. Mössbauer spectroscopy

The Mössbauer spectra were obtained in a transmission spectrometer at low temperature. A source of ^{57}Co in a Rh matrix of nominally 50 mCi was used. Velocity calibration was performed against a 12-μm-thick α-Fe foil. All isomer shifts mentioned in this paper refer to the standard at 298 K. The spectra were evaluated using a least squares nonlinear computer-fitting program with constraints. Lorentzian lines were considered with equal widths for each spectrum component. The spectra were folded to minimize the geometric effects.

2.3. Catalytic test

The catalysts (300 mg, 0.5–0.8 mm particle diameter) diluted with glass particles of the same size at a ratio of 1:5, were tested in a fixed-bed quartz tubular reactor operated at atmospheric pressure. The feed was either a mixture of 2 vol% propane and 10 vol% oxygen, balanced with helium, or a C_2H_5OH:O_2:He mixture of 1:20.8:78.2. The total flow rate was 100 mL min^{-1} measured at room temperature. The temperature, measured with a coaxial thermocouple, varied between 150 and 420 °C, increasing in steps of 20 °C, for propane oxidation, and 70 and 325 °C, in steps of 10 and 5 °C, for ethanol oxidation. The data obtained at each temperature were the average of three steady-state measurements. The reactants and reaction products were alternately analyzed on-line by gas chromatography. The conversion of VOC, $X\%$, is defined as the percentage of VOC feed that has reacted, that is,

$$X\% = \frac{(\mathrm{VOC})_{\mathrm{in}} - (\mathrm{VOC})_{\mathrm{out}}}{(\mathrm{VOC})_{\mathrm{in}}} \times 100.$$

Table 1
Results of specific surface area ($m^2\ g^{-1}$) of $LaCo_{1-y}Fe_yO_3$ calcined at 700 °C before and after catalytic test

Catalyst	SSA ($m^2\ g^{-1}$)	
	Fresh	Used
$LaCoO_3$	10.5	9.2[a]
$LaCo_{0.9}Fe_{0.1}O_3$	10.9	8.0
$LaCo_{0.7}Fe_{0.3}O_3$	14.3	13.9
$LaCo_{0.5}Fe_{0.5}O_3$	9.6	9.5
$LaFeO_3$	18.5	12.8[b]

[a] From Ref. [6].
[b] From Ref. [8].

3. Results

3.1. SSA

The SSAs of all of the catalyst series, measured before and after catalytic testing, are given in Table 1. The SSAs of $LaCoO_3$ and $LaFeO_3$ are also shown as references. After catalytic testing, the SSAs increased slightly, but the final values are in a small range that can be considered within the limits of experimental error.

3.2. XRD

Fig. 1 shows diffractograms of the $LaCo_{0.9}Fe_{0.1}O_3$ catalyst precursor without calcine as a function of temperature. Compared with the previous results for $LaCoO_3$ [6], here formation of the perovskite phase starts at 550 °C. At higher temperatures, an increase in the intensity of the crystalline diffraction lines is observed.

Fig. 2 shows diffractograms corresponding to the complete series of the catalysts calcined at 700 °C. Analyzing these diffractograms leads to four relevant observations:

1. In the detail of Fig. 2, the diffraction line at approximately 48° (2θ) is observed. An almost linear shift toward lower angles with increasing iron content is seen.
2. $LaCoO_3$ and $LaFeO_3$ reference perovskites have rhombohedral and orthorhombic structures, respectively. To identify each structure from the analysis of the main diffraction line is simple. For othorrombic structures, the main peak is single; for rhombohedral structures, it is split. As shown in the detail of Fig. 2, the most intense diffraction line ($2\theta \cong 33°$) is a doublet for all of the samples. Then the inclusion of different Fe amounts does not modify the perovskite rhombohedral structure.
3. The diffractogram is very clear, and the signal-to-noise ratio is high. The measurement was made at very low scan speed, 0.02°, at a counting time of 5 s per step. Diffraction lines of cobalt oxide and iron oxide (JCPDS files 2-770 and 33-664, respectively) are not observed. Although it can be considered noise, a peak where the main line of the La_2O_3 is assigned seems to begin to show.
4. The intensity changes are very small and random and are likely due to the amount of sample analyzed, as a conse-

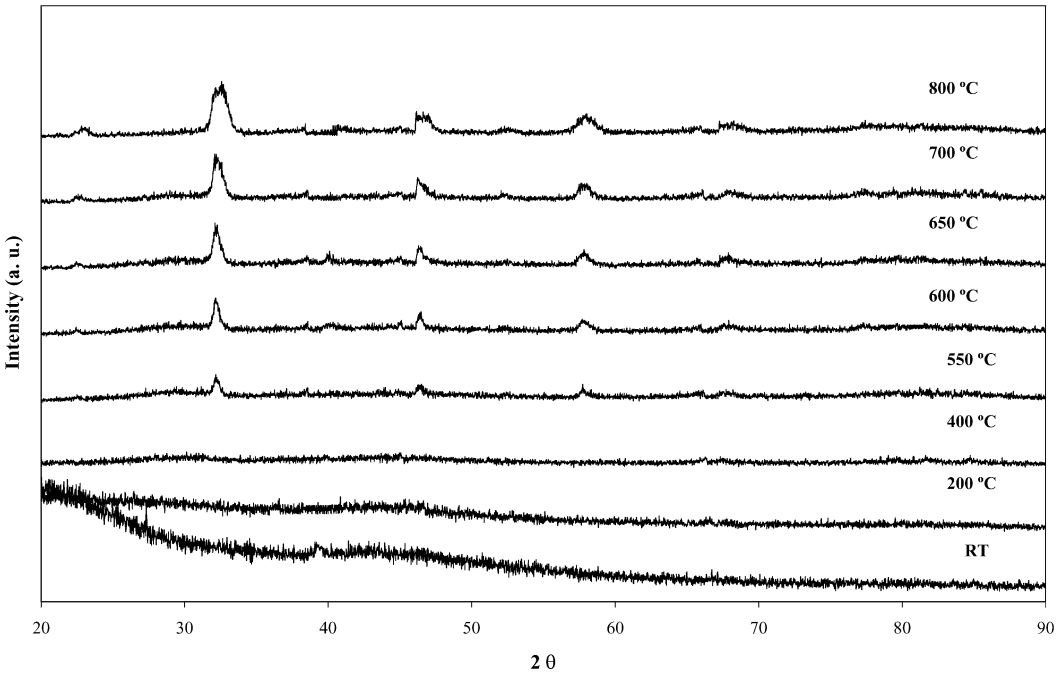

Fig. 1. XRD profiles of $LaCo_{0.9}Fe_{0.1}O_3$ at different calcination temperatures.

quence of the varying compression of the powder in the sample holder.

Crystallization of the perovskite structure begins at 550 °C, similar to that for $LaCoO_3$ perovskite [6]. Taking into account the similarity of these results and considering that for $LaCoO_3$, a notable decrease in the SSA was observed when the calcination temperature was increased from 700 to 800 °C, the $LaCo_{1-y}Fe_yO_3$ perovskites prepared in this work were calcined to 700 °C.

3.3. Drifts

Fig. 3 presents the DRIFTS spectra of the $LaCo_{1-y}Fe_yO_3$ perovskites. All exhibit one strong and well-defined absorption band at 567 cm^{-1}, with a shoulder at 623 cm^{-1}, typical of perovskite oxides ABO_3 [15–17]. The vibrational behavior of these materials is expected to be rather complex, taking into account that the crystal lattice is built up from two different metal oxygen polyhedra, one of which contains metallic cations of different charges and sizes. On the other hand, symmetry reduction observed in many of the materials investigated allows the prediction of additional spectral complexities.

Because both the B and B′ cations are present as octahedral BO_6 building blocks, strong vibrational coupling between them may be expected. On the other hand, the B–O bonds of these units, which involve metal cations of charges ranging between +3 and +6, are undoubtedly stronger than those belonging to the 12-coordinated A-O units. Based on this simple argument, the BO_6 units can be expected to behave as approximately "isolated" groupings that dominate the spectroscopic behavior. In some cases, if the charges and/or masses of the B and B′ cations differ significantly, then it should be possible to make some additional differentiation between BO_6 and $B'O_6$ vibrators [17]. The bands in the 500–730 cm^{-1} region are assigned to the stretching modes of the BO_6 octahedra. DRIFTS spectra of $LaCo_{1-y}Fe_yO_3$ exhibit an intense band at around 567 cm^{-1} with a shoulder at 623 cm^{-1}. The main band can be assigned to antisymmetric stretching vibration of the BO_6 octahedra [16,17], whereas the shoulder can be assigned to the symmetric stretching vibrations of these octahedra.

Both the intensity and the shift toward higher wavenumbers increase with increasing iron content, indicating weakening B–O bonds. A band at around 877 cm^{-1} appears, the intensity of which increases slightly with increasing iron content. As proposed by Berger et al. [18], this band may be related to structural modifications associated with Fe^{4+} formation. In this way, the band at 877–900 cm^{-1} would be related to the increased force constant of the Co–O bond.

3.4. XPS

The peak corresponding to Co_{2p} is characteristic of the Co^{3+}, which has a binding energy of 779.7 eV. First, it is possible to discard the presence of Co^{2+}, because satellite peaks at around 787.5 ± 0.5 eV are not observed in any of the catalyst spectra. No shifts of the binding energy of the Co_{2p} signal are observed either after changes in the iron content or after catalytic testing.

The Fe_{2p} binding energy is 710.1 ± 0.1 eV for all of the catalysts independent of Fe content. Analyzing the Fe_{2p} peak to determinate different oxidation states is difficult, because of Co Auger peak overlaps it. Therefore, it is necessary to make a deconvolution that includes the Co Auger peak.

Table 2 shows the surface atomic ratios obtained from the XPS results. The Fe/Co ratios with the Fe content in $LaCo_{1-y}Fe_yO_3$ ($y = 0.1, 0.3, 0.5$) follow the progressions 0.1, 0.6, and 0.9 for the fresh catalysts and 0.1, 0.5, and 0.8 for

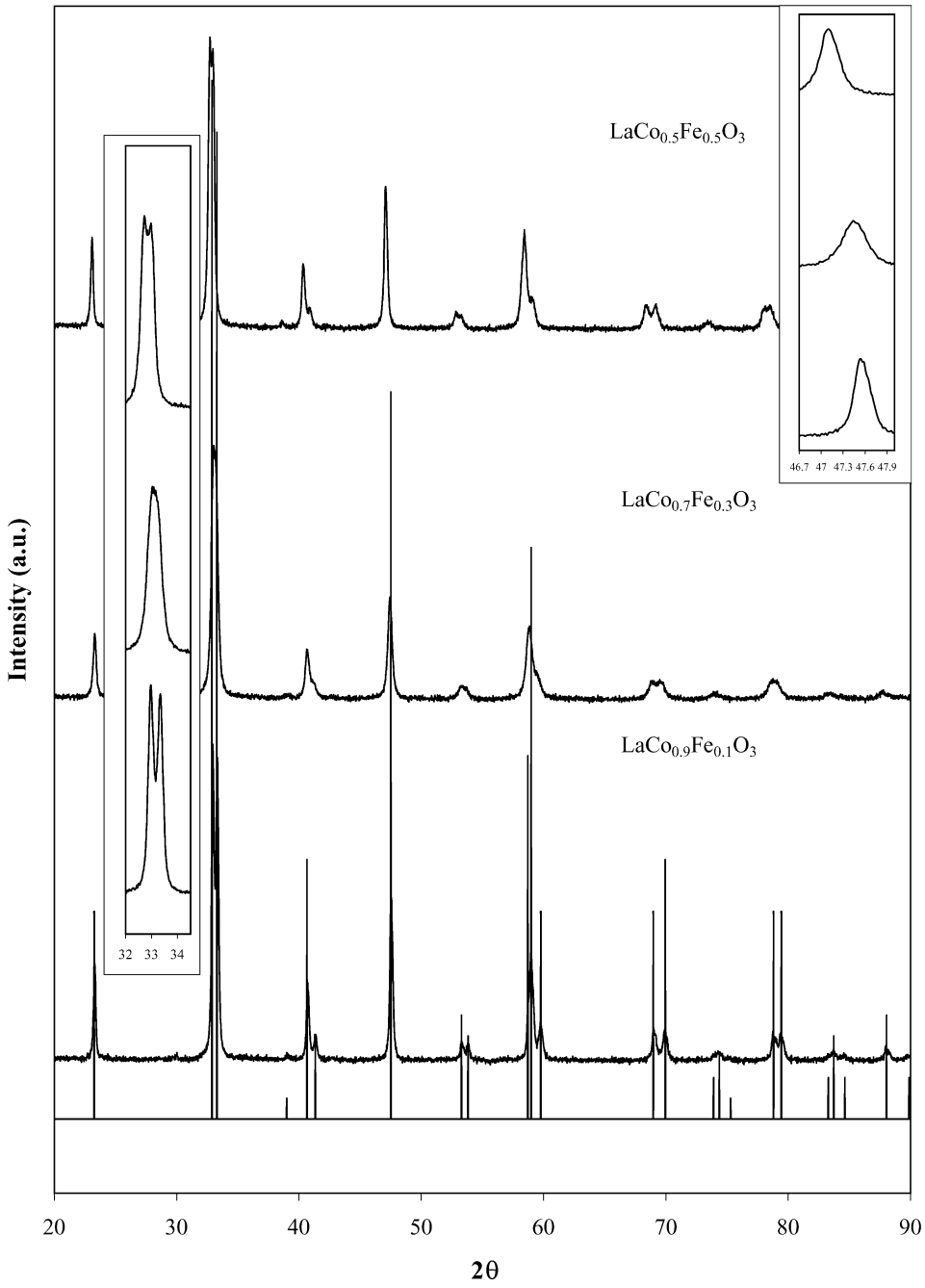

Fig. 2. XRD profiles of $LaCo_{1-y}Fe_yO_3$ ($y = 0.1, 0.3, 0.5$) calcined at 700 °C.

the used catalysts. The Fe/Co ratios for $LaCo_{1-y}Fe_yO_3$ perovskites with $y = 0.1$ and 0.3 are in good agreement with the nominal values, 0.11 and 0.43, respectively. The Fe/Co ratio from $LaCo_{0.5}Fe_{0.5}O_3$ is rather lower than the theoretical one. The small differences between before and after catalytic test can be attributed to the calculus error of the Fe concentrations induced by the overlapping with the Co Auger signal previously mentioned. It is important to note that the deviations from the nominal values are within ±10%.

The La/(Co + Fe) ratios are similar to those obtained with the $LaCoO_3$ perovskite (2.31 and 2.30 for fresh and used catalyst, respectively [6]), and a slight increase in Fe content from 2.0 to 2.3 is observed. This ratio is not modified after catalytic testing in propane oxidation.

The C/(La + Co + Fe) surface atomic ratios before and after catalytic testing are practically identical, indicating that the catalysts efficiently remove the carbon wastes under the operational conditions of this work.

3.5. Mössbauer spectroscopy

Fig. 4a shows spectra corresponding to a sample of $LaCo_{0.5}Fe_{0.5}O_3$ and a sample of hematite measured at 298 K. Fig. 4b presents the spectrum of $LaCo_{0.5}Fe_{0.5}O_3$ at 24 K. The spectra

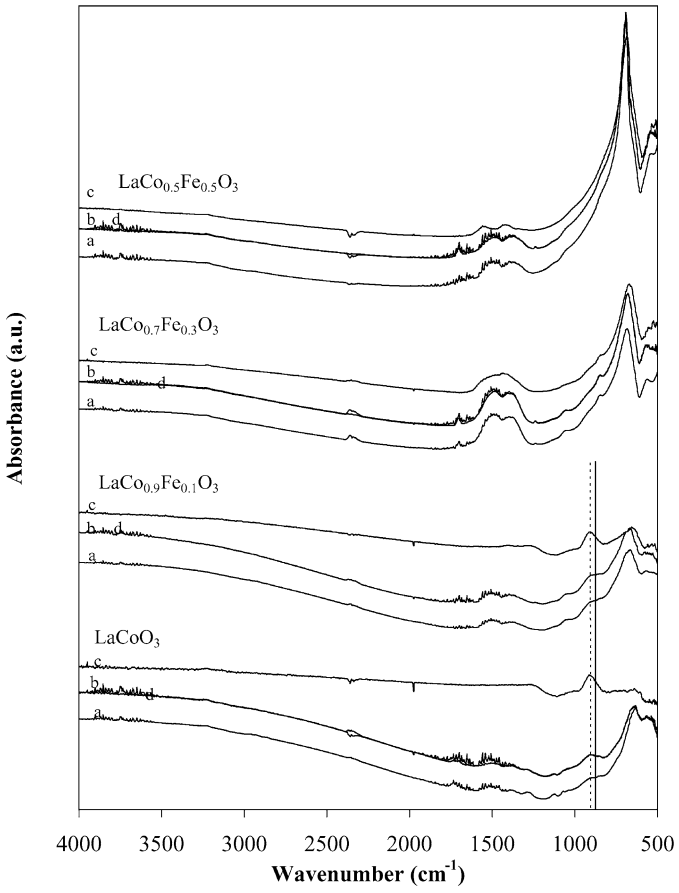

Fig. 3. DRIFT spectra of $LaCo_{1-y}Fe_yO_3$ ($y = 0.1$, 0.3, 0.5). (a) Samples at room temperature in air during 10 min. (b) Samples at room temperature in He flow for 10 min. (c) Samples at room temperature in He flow for 1 h, and (d) samples at 250 °C in He flow for 30 min.

of the samples with lower iron content are of very low intensity and thus are not analyzed or presented here.

The spectrum collected at 298 K is totally collapsed, and only a singlet is observed. Even so, this spectrum does not supply information about the various iron species and their relative content. Consequently, this spectrum was collected at 24 K, far below magnetic order temperature.

The data obtained at 24 K were fitted following the criteria used by Russo et al. [19] for $LaMg_{0.5}Fe_{0.5}O_3$. Therefore, three typical sextets of Fe^{3+} ions, assuming 0, 2, and 3 Co ion neighbors, were considered. Furthermore, a fourth sextet with hyperfine parameters assigned to Fe^{4+} ions and a singlet corresponding to paramagnetic or superparamagnetic Fe^{3+} were included in the fitting. The hyperfine parameters are given in Table 3. To maintain coherence with the fitting of the spectrum collected at 24 K, a singlet corresponding to Fe^{4+} ions was included in the fitting of the spectrum at 298 K.

3.6. TPR

TPR diagrams of all of the catalysts are presented in Fig. 5. As mentioned by Ciambelli et al. [20] and Barbero et al. [8], the Fe^{3+} would not be reduced under the experimental conditions of the TPR measurement. Only the reduction of Fe^{4+} to Fe^{3+} would be expected if there were Fe^{4+}. Then, because Co would be the cation to reduce in these conditions, it is not stranger that the reduction temperatures observed are similar to those of the $LaCoO_3$ perovskite and at approximately 395 and 600 °C [6]. The first peak, which is split for the $LaCoO_3$ perovskite, becomes a single peak when the Fe substitution increases. At high temperatures (∼670 °C), a peak can be observed at which intensity decreases with the Fe content until disappears for $LaCo_{0.5}Fe_{0.5}O_3$. The reduction of Fe^{4+} in substituted lanthanum orthoferrites has been detected at 355–385 °C [8,20,21]. This signal is in the same range as the first reduction signal of $LaCoO_3$ perovskite. Thus, the reduction temperature of Co^{3+} to Co^{2+} avoids detecting the reduction of Fe^{4+}, if it occurs. The second peak of the reduction of $LaCoO_3$ has been attributed to the reduction of Co^{2+} to Co^0 [22,23].

Table 2
XPS surface atomic ratios of $LaCo_{1-y}Fe_yO_3$ calcined at 700 °C before and after propane catalytic test

Catalyst	Fe/Co		La/(Co + Fe)		C/(La + Co + Fe)	
	Fresh	Used	Fresh	Used	Fresh	Used
$LaCo_{0.9}Fe_{0.1}O_3$	0.09	0.10	2.00	2.00	2.08	1.46
$LaCo_{0.7}Fe_{0.3}O_3$	0.66	0.48	2.30	3.00	2.14	1.88
$LaCo_{0.5}Fe_{0.5}O_3$	0.88	0.82	2.20	2.20	1.89	1.37

Table 3
Hyperfine parameters of $LaCo_{0.5}Fe_{0.5}O_3$ at 24 K

Species	H (kG)	δ (mm s^{-1})	2ε (mm s^{-1})	%
Fe^{3+} site 1 (0 Co)	519 ± 2	0.43 ± 0.02	−0.08 ± 0.02	35 ± 3
Fe^{3+} site 2 (2 Co)	484 ± 2	0.48 ± 0.02	−0.10 ± 0.02	36 ± 3
Fe^{3+} site 3 (3 Co)	442 ± 4	0.49 ± 0.04	−0.18 ± 0.04	16 ± 2
Fe^{4+}	256 ± 8	0.2 ± 0.1	−0.2 ± 0.1	7 ± 2
Paramagnetic and/or supermagnetic Fe^{3+}	–	0.36 ± 0.06	–	6 ± 1

3.7. Catalytic activity

Fig. 6 shows the temperature corresponding to 50% VOC conversion, T_{50}, as a function of Fe content. This parameter is a good indicator of catalytic activity and facilitates the comparison of different catalysts. $LaCoO_3$ and $LaFeO_3$ perovskites are shown as references.

A 10% substitution of Fe for Co improves catalytic performance in propane combustion. Higher Fe substitution levels increase the T_{50} in a practically linear way. The T_{50} value for $LaCo_{0.9}Fe_{0.1}O_3$ is the lowest and is similar to that obtained previously for $La_{0.6}Ca_{0.4}CoO_3$ [6].

The behavior for ethanol combustion is similar to that for propane combustion; however, in this case, the increased amount of Fe increases the T_{50} with a smaller ΔT. The 10% substitution of Fe for Co is sufficient to reach the catalytic performance showed by $La_{0.5}Ca_{0.5}CoO_3$ perovskite [6]. In fact, 10% Fe substitution maintains catalytic performance, whereas increasing the substitution level (to 50%) provokes decreased catalytic performance.

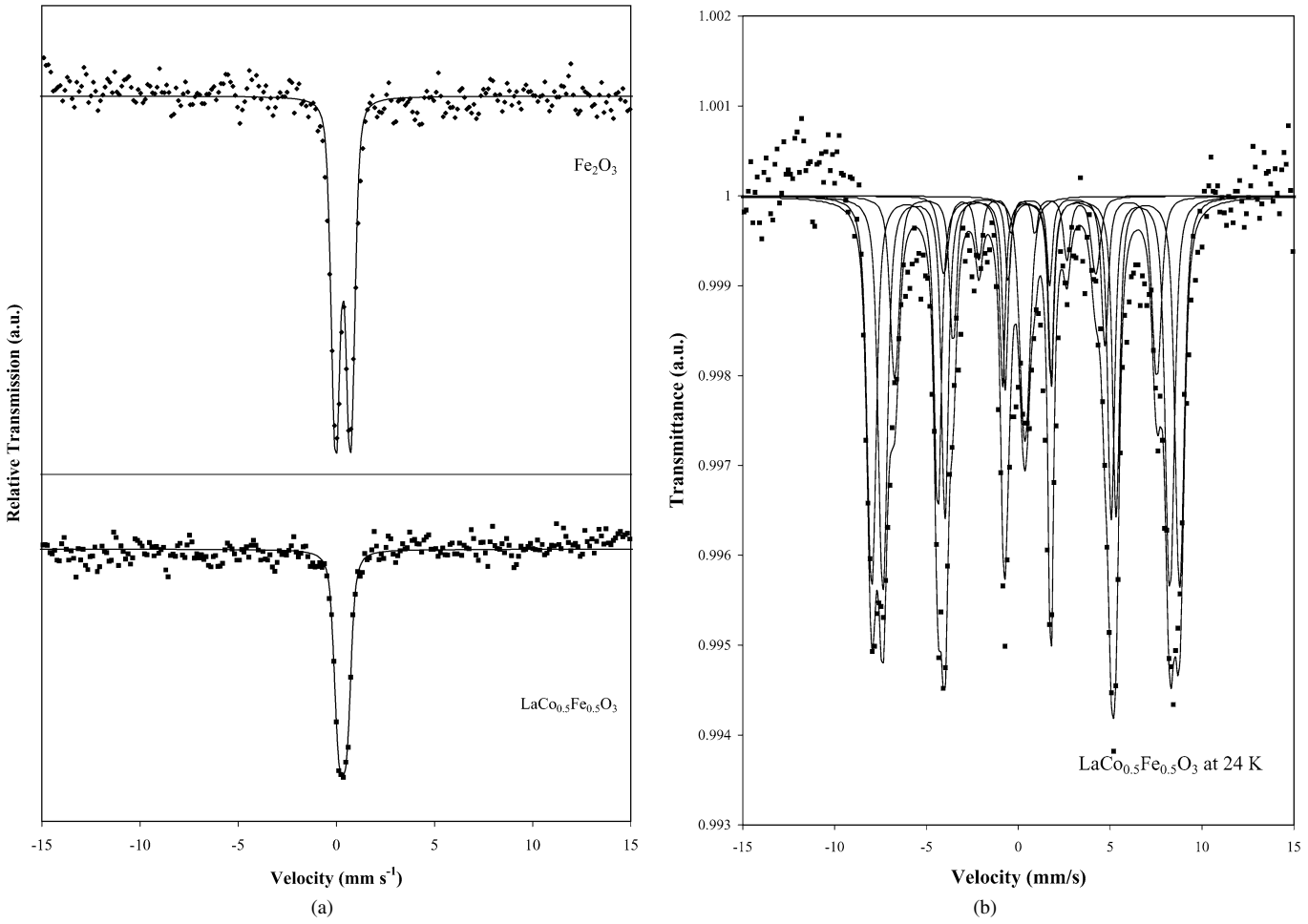

Fig. 4. (a) Mössbauer spectra for $LaCo_{0.5}Fe_{0.5}O_3$ perovskite and a sample of hematite measured at 298 K. (b) Mössbauer spectrum for $LaCo_{0.5}Fe_{0.5}O_3$ perovskite measured at 24 K.

4. Discussion

The main idea behind this work is to substitute Fe for Co in $LaCo_{1-y}Fe_yO_{3\pm\lambda}$ perovskites, to study Fe's stabilization effect in the structure. The synthesis method should guarantee not only the purity of the required phase, but also the suitable textural characteristics for a material to be used as catalyst. The maximum "y" value was selected based on the idea of substituting of Fe for Co, and not vice versa. To assign a role to the substituting cation in a material with a well-defined structure like the perovskites, the material should be pure, not a mixture of phases. Based on this requirement, the first point to be discussed is the kindness of the synthesis method and the structural consequences from the substitution.

4.1. Synthesis of a single perovskite phase: Structure and stoichiometry

The SSAs given in Table 1 show that the values obtained in both substitution extremes are similar to those reported for $LaCoO_3$ [3], which was synthesized using the same method. This may be due to the synthesis method (sol–gel citrate) or to the parameter control of the synthesis process. Goldwasser et al. [24] obtained 50% lower SSAs with a high dispersion of the values, with no relationship to the amount of Fe. Bedel et al. [25], by decomposition of propionates and calcining at 700 °C, obtained much lower SSAs than ours, 4 $m^2\,g^{-1}$ for $LaCoO_3$ and 9 $m^2\,g^{-1}$ for $LaFeO_3$.

As in our previous work [6], here the crystalline progression as a function of the calcination temperature was studied by in situ XRD. The perovskite structure crystallization begins at 550 °C, similar to that observed for $LaCoO_3$ perovskite [6]. Taking into account the similarity of these results and that for $LaCoO_3$, a notable decrease in SSA was observed when the calcination temperature was increased from 700 to 800 °C, the $LaCo_{1-y}Fe_yO_3$ perovskites prepared in this work were calcined to 700 °C. The similar SSAs obtained for the perovskites with and without iron indicate that the unsubstituted perovskite texture is not significantly modified by inclusion of iron. In fact, these data provide a clue that Fe is included in the structure of the $LaCoO_3$ perovskite without difficulty and, apparently, without modifying its structure. The XRD results of the samples calcined at 700 °C confirm this assumption (Fig. 2).

In all cases, the diffraction lines corresponding to the JCPDS 25-1060 file are observed, and these are assigned to the rhombohedral structure of the $LaCoO_3$ perovskite. However, due to the detection limits of the XRD technique, the segregation of iron and cobalt oxides cannot be completely discounted. In all

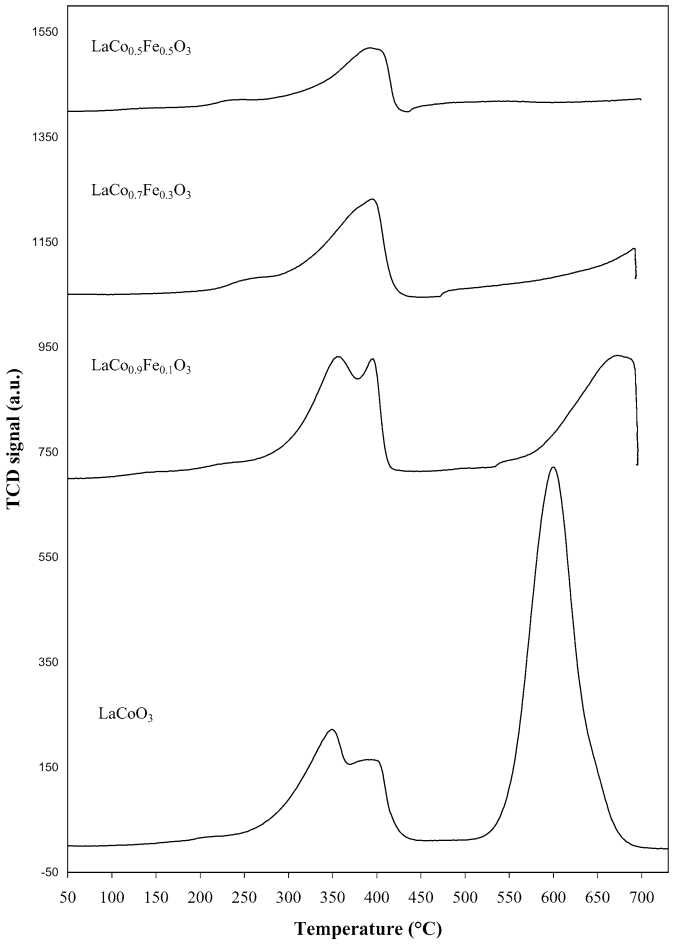

Fig. 5. TPR profiles of $LaCo_{1-y}Fe_yO_3$ ($y = 0.1, 0.3, 0.5$) calcined at 700 °C.

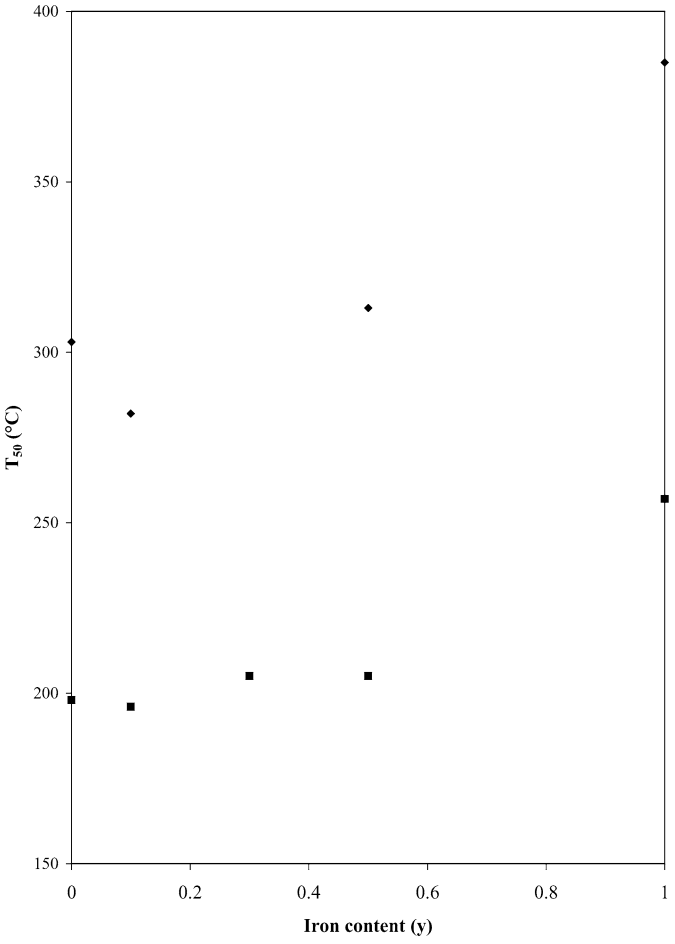

Fig. 6. T_{50} curves of $LaCo_{1-y}Fe_yO_3$ ($y = 0$ [6], 0.1, 0.3, 0.5, 1 [8]) in propane (◆) and ethanol (■) combustion.

of the diffractograms, a very weak signal a $2\theta \approx 30°$ is detected, which could correspond to the most intense diffraction line of La_2O_3 (JCPDS 5-602 file). After catalytic testing, a slight decrease in diffraction line intensity without the presence of new phases is observed.

Considering the extremes of the $LaCo_{1-y}Fe_yO_3$ perovskite series, $LaCoO_3$ (rhombohedral) and $LaFeO_3$ (orthorhombic) [6,8,25], the partial substitution of Fe for Co could lead to structural changes. Differentiation between the two possible structures is simple and can be done by analyzing the main diffraction line. This line is a doublet in the rhombohedral structure and single in the orthorhombic one. The diffractograms show that although the doublet of the main line tends to be a single line as the amount of Fe increases, the structure remains rhombohedral. This observation is in agreement with findings of Bedel et al. [25], who defined an Fe content limit of 50%, above which the structure becomes orthorhombic.

Although the structure is conserved in the range of Fe substitution, a notable shift of the diffraction lines toward lower 2θ angles with increasing Fe content is observed. This shift is practically linearly correlated with Fe content and it is originated by the expansion of the unit cell. This expansion could be explained by comparing the ionic radii that can exist in the structure. The Co^{3+} and Fe^{3+} ionic radii are 0.61 and 0.645 Å, respectively [26]. The values of Co^{3+} and Fe^{3+} are very close but sufficiently different to provoke expansion of the unit cell.

Table 4
Lattice parameters and ions occupancies of $LaCo_{1-y}Fe_yO_3$ perovskites from Rietveld method

Catalysts	a (Å)	α (°)	V (Å^3)	O occupancy	La occupancy
$LaCo_{0.9}Fe_{0.1}O_3$	5.386	60.7	112	0.99	1[a]
$LaCo_{0.7}Fe_{0.3}O_3$	5.416	60.6	114	0.98	1[a]
$LaCo_{0.5}Fe_{0.5}O_3$	5.439	60.6	115	0.99	1[a]

[a] Without refinement.

The expansion of the crystalline unit cell is corroborated by structure refinement using the Rietveld method, as shown in Table 4. The higher volume of the unit cell could be correlated with decreased strength of the B–O bond. In fact, the DRIFTS results are coherent with the XRD findings and indicate a shift of the band at 665–693 cm^{-1} toward higher wavenumbers with increasing Fe content. This shift indicates a weakening of the B–O bond, which could have consequences on both the reconstruction mechanism of the catalyst and its efficiency under reaction conditions.

Other relevant factors to consider when assigning the sites or active centers responsible for catalytic activity is the pu-

rity grade obtained with a particular synthesis method. Among the possible phases that could segregate are the oxides of the cations constituting the perovskite. Evaluation of the XRD results indicates probable segregation of only La_2O_3 by identifying its most intense diffraction line. However, due to the technique detection limitations, the possible existence of other oxides cannot be discounted. Several different characterization techniques were used in an attempt to identify other oxides as contaminants, including specific essays for each case.

Mössbauer is a very sensible technique for detecting free Fe_2O_3. All of the catalysts show similar isomeric shifts (δ) within the error bands that correspond to Fe^{3+}. Analysis of the quadrupolar splitting values (Δ) revealed that they are very small or nonexistent. This parameter gives an idea of the site symmetry where the ion is found. Because Fe^{3+} is d^5, if there was an isolated ion, then this value should be $\Delta = 0$. In practice, however, distortions or asymmetric surroundings that produce $\Delta \neq 0$ always exist. In the case of hematite with very small crystallite sizes (shown in Fig. 4a), as expected for our catalysts because they are not detected by XRD, a doublet is obtained at room temperature, but with Δ on the order of 0.8 mm s^{-1}. Evidently, this is not the case for our catalysts (Fig. 4a), which seem to have ions in very symmetric surroundings, and so the existence of hematite can be discarded. According to the nominal synthesis values, the Fe/Co atomic ratios should be 0.11, 0.43, and 1.00. The values obtained by XPS follow this progression with increasing Fe content. Only for $y = 0.5$ is a Fe/Co XPS ratio 10% lower than the theoretical one observed; thus, any phase rich in iron would have segregated to the surface, and all of the iron would have been incorporated into the perovskite structure. Moreover, the La/Co + Fe atomic ratio is 2.3, similar to the La/Co atomic ratio obtained for $LaCoO_3$ (2.31 for fresh and 2.30 for used catalyst [6]). This indicates that substituting Co for Fe does not alter the superficial enrichment of La.

The La excess at the surface, studied previously [6,27], and may or may not imply the existence of La_2O_3. The DRIFTS spectra show the existence of vibrational modes in the range that could be identified as carbonates. The probable presence of free lanthana in a CO_2-rich atmosphere would result in the formation of lanthanum carbonate. Because of this, and to discriminate this signal of probable contamination with CO_2 from the working atmosphere, the sample was first analyzed in an air atmosphere, then in an atmosphere with CO_2, and finally in an inert atmosphere of He, with increasing treatment temperature (Fig. 7). On treatment at 250 °C in He atmosphere, the bands at 1400–1600 cm^{-1} decrease in intensity without totally disappearing. On treatment in CO_2 atmosphere at 350 °C and the subsequent purge with inert gas, the signal intensity does not increase. The intensity of the band assigned to the carbonates is low, and it can be supposed that if free La_2O_3 exists, it is present only in very small amounts, in agreement with the XRD findings.

It can be concluded that the citrate synthesis method, with proper control of the dry and calcination parameters, yields high-purity perovskites with excellent textural characteristics to be used as catalyst in combustion of VOCs. Yet a slightly La superficial excess could lead to the formation of La_2O_3 at

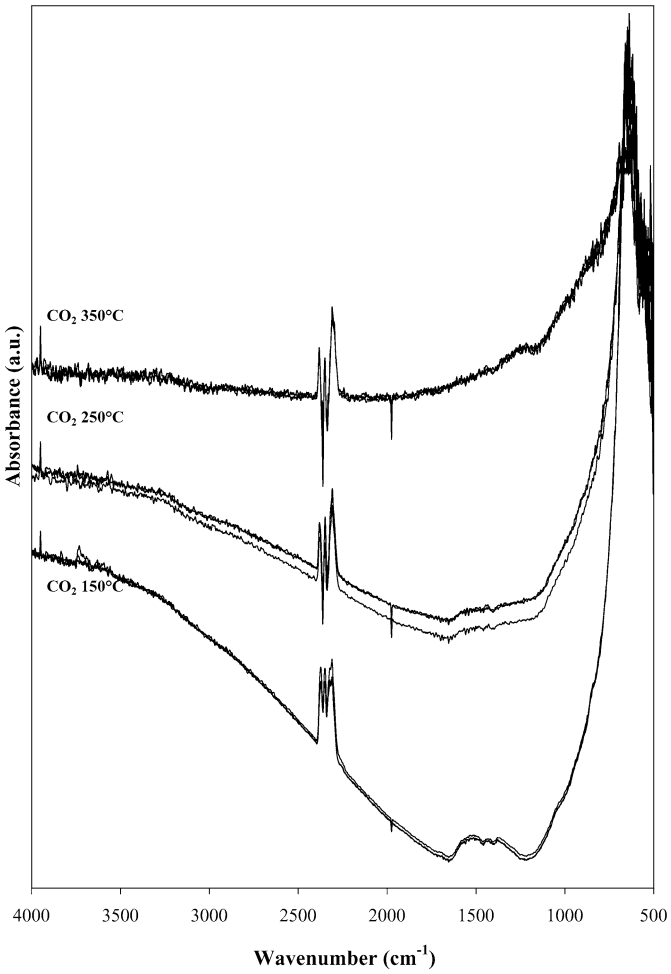

Fig. 7. DRIFT spectrum of $LaCo_{0.9}Fe_{0.1}O_3$ in CO_2/He flow, at 150 °C (1 min, 30 min, 60 min), 250 °C (1 min, 30 min, 60 min), 350 °C (1 min, 30 min, 60 min).

trace levels. This conclusion is in agreement with the results obtained by O'Connell et al. [27], who reported a lower than nominal La/Co surface atomic ratio for $LaCoO_3$ perovskites. Inclusion of iron in the $LaCoO_3$ perovskite structure is tolerated in the studied range, and the main structural consequence is an expanded crystalline cell size. This expansion is assigned to the relative size of the Fe^{3+} cation compared with the Co^{3+} cation, although the possibility that it will be reduced by the presence of Fe^{4+} (which has lower relative ionic radius) at high iron content cannot be discounted. Furthermore, a weakening of the B–O bond coincides with the expansion of the unit cell and has no effect on crystalline organization, preserving the rhombohedral structure of the $LaCoO_3$ perovskite.

4.2. Structural stability

Increasing the amount of Co in the $La_{0.9}Ce_{0.1}Co_{1-x}Fe_xO_3$ perovskite leads to decreased structural stability [7]. In addition, and discussing the structure type, Bedel et al. [25] mentioned that up to a 50% substitution of Fe for Co, the structure remains rhombohedral, and on greater substitution, the structure becames orthorhombic. In fact, these are the crystalline

structures of the $LaCoO_3$ and $LaFeO_3$ perovskites, respectively. Bedel et al. [25] have established a relationship between crystalline structure and structural stability. Despite this, as described in the previous section, up to the substitution levels of Fe for Co that have been studied in this work, no structural modification occurs, so it would have to deepen in the study of the transformations that promote stability.

Both the specific surface area and the XPS Co/Fe ratio data, before and after catalytic testing, suggest that the catalysts are stable or achieve improved stability due to the incorporation of iron into the structure. SSAs $\geqslant 10\ m^2\ g^{-1}$ are higher than those reported for other synthesis methods and are difficult to maintain. Even $LaFeO_3$ perovskite treated under rigorous reduction conditions (5% H_2/N_2 and $T_{max} = 700\,^{\circ}C$) preserves the Fe from its total reduction to Fe^0 [8]. At higher temperatures (e.g., 900 °C), its total reduction would be possible. In contrast, in similar conditions $LaCoO_3$ perovskite is destroyed and Co^0 is formed, expulsing it from the structure [6]. However, it is notable that these perovskites can be rebuilt by reoxidation. This fact is an excellent indicator of potential structure stability, because the working atmosphere is slightly oxidant. A combination of factors can a priori indicate that incorporation of Fe into the base structure with Co could improve the structural stability needed for an exigent catalytic process like VOC combustion, where the catalysts support high temperatures under H_2O and CO_2 atmosphere.

TPR results can give important information if the products of the catalyst reduction are analyzed by XRD. TPR diagrams are shown in Fig. 5. In $La_{1-x}Ca_xFeO_3$ perovskites, Barbero et al. [8] observed a peak at ∼355 °C whose intensity increases with increasing Ca content. The peak at low temperatures is assigned to the Fe^{4+} transition to Fe^{4+}/Fe^{3+}; the second one, to Fe^{4+}/Fe^{3+} toward Fe^{3+}. If Co were present, then both peaks would be masked by the reduction of Co^{3+} to Co^{2+}, which is established in the temperature range of 150 °C to ∼450 °C [6], although any peak between 200 and 300 °C is observed when calcium is not present. The peak at ∼240 °C is evident only in the perovskite with higher Fe content, and it could indicate the existence of Fe^{4+} for this degree of substitution for Co. The incorporation of Fe affects the first reduction stage, modifying the split peak of the $LaCoO_3$ perovskite and showing only one peak, probably avoiding an intermediate reduction state. The reduction diagram is also modified with the Fe content in the second reduction peak at ∼670 °C. This peak, assigned to the reduction of Co^{2+} to Co^0 [6], decreases in intensity with increasing Fe amount and disappears when the level of substitution reaches 50%. Despite this, the peak can also be attributed to the reduction of Fe^{n+} to Fe^0. To make this happen, as discussed previously for $LaFeO_3$ perovskite [8], the iron should be present as free iron oxide outside the perovskite structure. In Section 4.1 the presence of free Fe_2O_3 was discarded. Therefore, only the Co reduction and a decrease in the hydrogen consumption with the increasing iron content could be expected. Consequently, the analysis of the catalysts' XRD diffractograms after TPR could be expected to help clarify these results.

$LaCo_{1-y}Fe_yO_3$ perovskites have been characterized due to their great stability, demonstrated mainly in the preservation of the perovskite structure as determined by XRD, even after such aggressive treatment as reduction with a 5% hydrogen flow at high temperature. The diffractograms are shown in Fig. 8. Two important observations can be made:

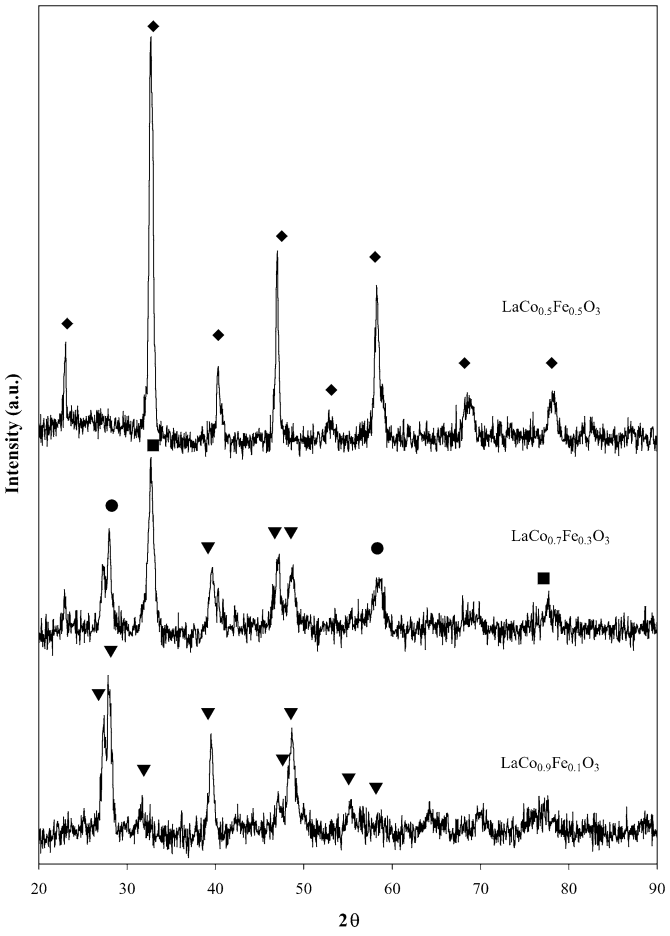

Fig. 8. XRD profiles of $LaCo_{1-y}Fe_yO_3$ ($y = 0.1, 0.3, 0.5$) after TPR. JCPDS files: (◆) 40-224 $LaCo_{0.4}Fe_{0.6}O_3$, (●) 2-770 Co_2O_3, (▼) 22-369; 5-602; 22-641 La_2O_3 and (■) 33-664 Fe_2O_3.

1. Only a 10% substitution of iron for cobalt is sufficient for the decomposition of perovskite to lead to the production of Co_2O_3 before Co^0. Only Co^0 traces would be produced. Moreover, the existence of a residual perovskite containing Co and Fe is observed.
2. The system has the ability to almost totally preserve the perovskite structure when the amount of substituted Co increases. These observations can explain the intensity decrease in the second peak of the TPR diagram, because the Co would be reduced only from +3 to +2.

It also can be concluded that the incorporation of Fe plays an important role in the preservation of the perovskite structure avoiding Co segregation, and even if segregated, the iron could prevent total Co reduction. As an additional consequence, the iron shifts the first stage of the cobalt reduction to higher temperatures. The capacity of the iron to preserve the perovskite structure, even in the orthorhombic $LaFeO_3$ and in the rhom-

bohedral $LaCo_{1-y}Fe_yO_3$ studied in this work, would indicate that the role of iron could be related to its capacity to activate or inhibit oxidant or reducing species and in this way preserve the host structure in which it exists. Thus, expansion of the unit cell volume provoked by the inclusion of iron is accompanied by weakening of the B–O bond and it does not have as a consequence a higher reducibility of the solid system, although it probably affects the capacity and the mechanism of oxygen supply and redox behavior.

4.3. Catalytic consequences

The aim of including iron in the perovskite structure is to stabilize the catalyst, but it is necessary to identify the catalytic role of the iron. In fact, a 10% Fe substitution maintains catalytic performance, but increasing the substitution level (up to 50%) provokes a decrease in catalytic performance. Considering that the desired effect of including iron in the structure is to add structural stability to the good catalytic performance, the fact that the T_{50} of the $LaCo_{0.9}Fe_{0.1}O_3$ perovskite is similar to that obtained with $La_{0.6}Ca_{0.4}CoO_3$ is an excellent result [6].

The results prompt two questions: (1) what is the cause of this observed singularity activity, and (2) in catalytic terms, given the characteristics that let us presume structural stability in rigorous reaction conditions, whether these catalysts are stable.

4.3.1. Catalytic behavior: Electronic implications

To explain what occurs with the singularity that provokes a small addition of iron, first it is important to understand the behavior of the cations involved and the possibilities that appear when there are two cations, Co and Fe, which can generate a redox-coupled pair that would exhibit redox behavior. Cobalt has two probable oxidation states, Co^{2+} and Co^{3+}, each of which can be high-spin or low-spin. The $Co_{2p_{3/2}}$ binding energy observed on XPS, 779.7 eV, is characteristic of Co^{3+}. The difficulty entailed in deconvoluting and analyzing the Co_{2p} components does not allow discrimination of Co^{2+} [28]. Despite this, the presence of Co^{2+} can be discounted because the satellite peak between 785 and 788 eV [27] is not observed in any catalyst. The analysis described at the beginning of Section 4 and the observation that the expansion of the unit cell can be explained by the larger size of the Fe^{3+} cation compared with Co^{3+} allow us to discount the existence of Co^{4+}, whose ionic radium is much smaller than the one of the Co^{3+}, so it could have a contrary effect to that observed on the dimensions of the unit cell. Nevertheless, it is widely accepted in the literature that even with the existence of an electronic disbalance, due to the A substitution for a cation with a lower oxidation state, in $LaA'CoO_3$ perovskites there is no Co^{4+}, but instead oxygen vacancies are generated. In addition, analysis of the Fe_{2p} peak is difficult because the Auger Co peak overlaps it, so a decomposition that includes both cations is necessary. This could have affected the accuracy of the data. The La/(Fe + Co) surface atomic ratio obtained from XPS clearly indicates an La surface excess outside the structure. This ratio increases slightly (from 2 to 2.3) with increasing iron content, indicating that in the $LaCo_{1-y}Fe_yO_3$ perovskites, the lanthanum outside the structure provokes an electronic disbalance that is compensated for at high iron content with part of iron in an unusual oxidation state, +4. The results obtained by Mössbauer spectroscopy confirm the existence of Fe^{4+}.

Following the methodology of Russo et al. [19] for $LaMg_{0.5}Fe_{0.5}O_3$ for the spectrum at 24 K, three sextets for Fe^{3+} were used, with 0, 2, and 3 Co as neighbors. It also appears a fourth sextet with parameters that can be assigned to Fe^{4+} and a singlet of Fe^{3+} paramagnetic or superparamagnetic. At 298 K the spectrum has completely collapsed, and only a doublet is observed. To maintain the coherence with a fit at 24 K, a single line corresponding to Fe^{4+} is shown in Fig. 4b. Table 3 gives the hyperfine parameters.

If the host structure, either orthorhombic or rhombohedral [29], is the determining factor in the deep Co reduction or the capacity for Co retention without being expulsed from the structure, then these observations cannot be related to the absence of Fe^{4+} in $LaFeO_3$ perovskite reported by Barbero et al. [8]. The DRIFTS spectra (see Fig. 3) show a band with varying intensity at 877–900 cm^{-1} in all of the catalysts, with the intensity increasing with the iron amount. As was proposed by Berger et al. [18], this band may be related to structural modifications associated with Fe^{4+} formation. In this way, the band at 877–900 cm^{-1} would be related to the increased force constant of the Co–O bond due to the presence of Fe^{4+}. Moreover, the Fe^{3+}–Fe^{4+} couple could play an important role in catalytic behavior. The La excess at the surface and its likely segregation in small amounts as La_2O_3 is observed in all of the studied series, and as has been mentioned by O'Connell et al. [27], this can be compensated for only by a change in the nominal ratio of the La and Co cations during synthesis. Petric et al. [30], through electric conductivity measurements of the $La_{1-x}Sr_xCo_{0.8}Fe_{0.2}O_{3-\delta}$ and $La_{0.3}Sr_{0.7}Co_{1-y}Fe_yO_{3-\delta}$ catalyst series, found two significant properties that can help explain our results. First, small amounts of Fe move the semiconductor behavior to metallic at high temperatures; Petric et al. assigned this to the stabilizing role of the Fe on high-spin Co^{3+}. From a second series, the authors concluded that increasing the Fe content produces a replacement of the dominant carrier. Dasgupta et al. [31] also observed for $Nd_{0.7}Sr_{0.3}Fe_{1-x}Co_xO_3$ perovskites an increase in conductivity with x. Therefore, it can be established that at low iron amounts, the stabilization of high-spin Co^{3+} will favor the existence of the Co^{3+}–Co^{III} couple (where Co^{III} are the Co ions in the low-spin state). When the Fe content is increased, charge compensation via Fe^{4+} formation would be produced and, according to observations of Tai et al. [32], the Fe^{4+}–Fe^{3+} couple would prevail over the Co couple. At low temperatures, the Co ions are mainly in their low-spin state. At high temperatures, Co^{3+} reaches a paramagnetic state of high spin. Heikes et al. [33], Raccah and Goodenough [34], and Bhide et al. [35] have reported that in $LaCoO_3$ perovskites, the Co charges are divided according to the following reaction:

$$2Co^{3+} \leftrightarrow Co^{2+} + Co^{4+}$$

Table 5
Results of the catalytic activity before and after hydrotreatment of $LaCo_{1-y}Fe_yO_3$

Catalysts	Temperature (°C)	X (%)[a]	X (%)[b]
$LaCoO_3$	180	25.7	19.1
	200	57.2	57.5
$LaCo_{0.9}Fe_{0.1}O_3$	180	19.1	28.7
	200	43.9	59.8
$LaCo_{0.7}Fe_{0.3}O_3$	180	17.1	15.3
	200	35.0	29.5
$LaCo_{0.5}Fe_{0.5}O_3$	180	17.0	19.3
	200	37.8	40.2
$LaFeO_3$	180	0.35	0.98
	200	0.79	5.1
	220	9.2	9.5

[a] Catalytic activity before hydrotreatment.
[b] Catalytic activity after hydrotreatment.

with an equilibrium constant

$$K_{\text{Disproportionation}} = \frac{[Co^{2+}][Co^{4+}]}{[Co^{2+}]} = \exp\left[-\frac{\Delta G_D^0}{RT}\right].$$

This phenomenon could occur in our catalysts at very low iron content, although neither Co^{2+} nor Co^{4+} would be observed.

Based on the foregoing findings, we can conclude that the singularity observed in the catalytic activity for $y = 0.1$ can be explained by the electronic complexity introduced by iron in the perovskite conductor. The appearance of Fe^{4+} would modify the redox-coupled pair responsible for controlling the electronic mobility in the perovskite.

4.3.2. Catalytic behavior: Structural stability

Finally, with the aim of proving the stability mentioned in the earlier discussion, the catalysts were studied under thermal hydrotreatment, simulating rigorous conditions of use. The experiment involved measuring catalytic activity at 180 and 200 °C using a reactive mixture C_2H_5OH:O_2:He=1:20.8:78.2 and a total flow of 100 mL min^{-1}. Then the catalyst was exposed to extreme conditions for 5 h, and finally catalytic activity was measured at the initial conditions. The extreme working conditions were as follows:

(i) Reaction temperature of 450 °C. This temperature is higher than that required for 100% conversion. According to the calculus for the reactor design, that would be the temperature of the combustion gases at the end of a fixed-bed reactor with the concentration and flows used in this study and from which the operative conditions have been selected.
(ii) Gaseous flow composition of CO_2:H_2O:He = 2:3:95 and total flow of 100 mL min^{-1}. This composition was chosen assuming complete conversion from the reactive mixture to water and carbon dioxide.

For reference purposes, Table 5 gives the results obtained with $LaCoO_3$ and $LaFeO_3$ perovskites.

As reported earlier [6], the activity of the $LaCoO_3$ perovskite decreases slightly after the first reaction cycle. After the hydrotreatment, the sample demonstrates a significant decrease in activity at low temperature (180 °C). At the other extreme, the $LaFeO_3$ perovskite does not show variations in catalytic performance. The comparison is made at 220 °C, the temperature at which the catalytic activity values detected can be trusted. These findings clearly indicate the potential role of Fe in structural stability.

Substituting Fe for Co does not provoke catalyst deactivation after hydrotreatment, but it does improve the catalytic performance. The improvement is more significant at low iron content and low reaction temperatures. This result agrees with the findings presented in Section 4.2. Moreover, it also agrees with those findings reported by Dasgupta et al. [31] related to the role of temperature and the weight of the electronic transport mechanism between the redox-coupled ions that can potentially act as active sites in the catalysts. Therefore, it is evident that more than one reaction mechanism occurs at different reaction temperatures and that these mechanisms likely coexist in a widely variable temperature range depending on which VOC is used as a reactant.

Thermal hydrotreatment at high temperatures demonstrate the importance of the reaction conditions on the definitive arrangement of the catalyst, resulting in a "positive aging." Further studies are needed to elucidate the details of what is occurring in the superficial physicochemistry of the catalyst.

5. Conclusion

The synthesis method of citrate, with proper control of the dry and calcination parameters, can produce high-purity perovskites with excellent textural characteristics. However, a slight La excess can lead to the formation of La_2O_3 traces. These perovskites' textural characteristics make them suitable for use as catalysts in the combustion of VOCs. The inclusion of iron in the $LaCoO_3$ perovskite structure is tolerated within the studied range, with the main structural consequence an expansion of the unit cell volume. This expansion is assigned to the relative size of the Fe^{3+} cation compared with the Co^{3+} cation, although at high iron content the expansion would be reduced by the presence of Fe^{4+}, which has a smaller relative ionic radius. Furthermore, a weakening of the B–O bond coincides with the expansion of the unit cell and has no effect on the crystalline organization. Moreover, the rhombohedral structure of the $LaCoO_3$ is preserved.

Fe plays an important role in preserving the structure, preventing Co segregation or shifting it to higher temperatures. Even when segregated, Fe can prevent the total reduction of Co by shifting the first stage of the cobalt reduction to higher temperatures. Fe's capacity to preserve the perovskite structure even in the orthorhombic $LaFeO_3$ and in the rhombohedral $LaCo_{1-y}Fe_yO_3$ studied in this work indicates a possible link to its ability of activate or inhibit oxidant or reducing species and preserve the host structure in which it is found. In this way, the expansion of the cell volume and the consequently weakening of the B–O bond, provoked by the inclusion of the iron, do not

have as a consequence a higher reducibility of the solid system, although they probably affect the capacity and the mechanism of oxygen supply or the redox behavior. At high iron content, Fe^{4+} could exist.

The singularity observed in the catalytic activity for $y = 0.1$ may be explained by the electronic complexity in the perovskite conductor characteristics introduced by the iron. The appearance of Fe^{4+} would modify the redox ion couple responsible for controlling the electronic mobility in the perovskite.

Hydrotreatment at high temperatures demonstrated the importance of the reaction conditions to the definitive arrangement of the catalyst, resulting in a "positive aging." It also showed that incorporating a small amount of iron can enhance the structural stability of the $LaCoO_3$ perovskite, which exhibits very good catalytic performance.

Acknowledgments

Financial support from CONICET, Universidad Nacional de San Luis, ANPCyT (Argentina) and SEPCyT (Argentina)–FNRS (Belgium) is gratefully acknowledged. The authors also thank Gustavo Marchetti (CINDECA, La Plata, Argentina) for the Mössbauer study, Julio Andrade Gamboa (Centro Atómico Bariloche, Argentina) for the Rietveld study, and Pierre Eloy and Caroline Cellier (Université Catholique de Louvain, Louvain la Neuve, Belgium) for their help with XPS and DRIFTS analyses, respectively.

References

[1] L.G. Tejuca, J.L.G. Fierro, J.M.D. Tascón, Adv. Catal. 36 (1989) 237.
[2] L. Forni, I. Rossetti, Appl. Catal. B 38 (2002) 29.
[3] H. Dai, H. He, P. Li, L. Gao, C. Au, Catal. Today 90 (2004) 231.
[4] P. Courty, H. Ajot, C. Marcilly, B. Delmon, Power Technol. 7 (1973) 21.
[5] S. Kaliaguine, A. Van Neste, V. Szabo, J.E. Gallot, M. Bassir, R. Muzychuk, Appl. Catal. A 209 (2001) 345.
[6] N.A. Merino, B.P. Barbero, P. Grange, L.E. Cadús, J. Catal. 231 (2005) 232.
[7] H. Tanaka, N. Mizuno, M. Misono, Appl. Catal. A 244 (2003) 371.
[8] B.P. Barbero, J. Andrade Gamboa, L.E. Cadús, Appl. Catal. B 65 (2006) 21.
[9] L.G. Tejuca, J.L.G. Fierro (Eds.), Properties and Applications of Perovskite-Type Oxides, Marcel Dekker, New York, 1993.
[10] L. Lisi, G. Bagnasco, P. Ciambelli, S. De Rossi, P. Porta, G. Russo, M. Turco, J. Solid State Chem. 146 (1999) 173.
[11] P. Ciambelli, S. Cimino, L. Lisi, S. De Rossi, M. Faticanti, G. Minelli, P. Porta, Appl. Catal. B 29 (2001) 239.
[12] J. Hermia, S. Vigneron, Catal. Today 17 (1993) 349.
[13] A. O'Malley, B.K. Hodnett, Catal. Today 54 (1999) 31.
[14] J.L.G. Fierro, J.M.D. Tascón, L. González Tejuca, J. Catal. 93 (1985) 83.
[15] S.D. Ross, Inorganic Infrared and Raman Spectra, McGraw–Hill, London, 1972.
[16] M. Couzi, P.V. Huong, Ann. Chim. 9 (1974) 19.
[17] A.E. Lavat, E.J. Baran, Vib. Spectrosc. 32 (2003) 167.
[18] D. Berger, V. Fruth, I. Jitaru, J. Schoonman, Mater. Lett. 58 (2004) 2418.
[19] U. Russo, L. Nodari, M. Faticanti, V. Kuncser, G. Filoti, Solid State Ionics 176 (2005) 97.
[20] P. Ciambelli, S. Cimino, L. Lisi, M. Faticanti, G. Minelli, I. Pettiti, P. Porta, Appl. Catal. B 33 (2001) 193.
[21] R. Spinicci, A. Tofanari, A. Delmastro, D. Mazza, S. Ronchetti, Mater. Chem. Phys. 76 (2002) 20.
[22] T. Nakamura, G. Petzow, L.J. Gauckler, Mater. Res. Bull. 14 (1979) 649.
[23] L. Wachowski, S. Zielinski, A. Burewixz, Acta Chim. Acad. Sci. Hung. 106 (3) (1981) 217.
[24] M.R. Goldwasser, M.E. Rivas, M.L. Lugo, E. Pietri, M.J. Pérez-Zurita, M.L. Cubeiro, A. Griboval-Constant, G. Leclercq, XIX Simposio Iberoamericano de Catálisis, México (2004) p. 78.
[25] L. Bedel, A.C. Roger, C. Estournes, A. Kiennemann, Catal. Today 85 (2003) 207.
[26] R.D. Shannon, Acta Crystallogr. A 32 (1976) 751.
[27] M. O'Connell, A.K. Norman, C.F. Hüttermann, M.A. Morris, Catal. Today 47 (1999) 127.
[28] M. Oku, Y. Sato, Appl. Surf. Sci. 55 (1992) 37.
[29] L. Forni, I. Rossetti, Appl. Catal. B 38 (2002) 29.
[30] A. Petric, P. Huang, F. Tietz, Solid State Ionics 135 (2000) 719.
[31] N. Dasgupta, R. Krishnamoorthy, K.T. Jacob, Mater. Sci. Eng. B 90 (2002) 278.
[32] L.W. Tai, M.M. Nasrullah, H.U. Anderson, D.M. Sparlin, S.R. Sehlin, Solid State Ionics 76 (1995) 273.
[33] R.R. Heikes, R.C. Miller, R. Mazelsky, Physica 30 (1964) 1600.
[34] P.M. Raccah, J.B. Goodenough, J. Appl. Phys. 39 (1968) 1209.
[35] V.G. Bhide, D.S. Rajoria, Y.S. Reddy, G. Rama Rao, G.V.Ž. Subba Rao, C.N.R. Rao, Phys. Rev. Lett. 28 (1972) 1133.